



## Aeolian dust supply from the Yellow River floodplain to the Pleistocene loess deposits of the Mangshan Plateau, central China: Evidence from zircon U-Pb age spectra



Yuan Shang <sup>a, b,\*</sup>, Maarten A. Prins <sup>b</sup>, Christiaan J. Beets <sup>b</sup>, Anu Kaakinen <sup>a</sup>, Yann Lahaye <sup>c</sup>, Noortje Dijkstra <sup>b, 1</sup>, Daniël S. Rits <sup>b</sup>, Bin Wang <sup>d</sup>, Hongbo Zheng <sup>e</sup>, Ronald T. van Balen <sup>b, f</sup>

<sup>a</sup> Department of Geosciences and Geography, P.O. Box 64, 00014, University of Helsinki, Finland

<sup>b</sup> Department of Earth Sciences, Faculty of Science, Vrije Universiteit Amsterdam, De Boelelaan 1085, 1081 HV, Amsterdam, The Netherlands

<sup>c</sup> Geological Survey of Finland (GTK), Betonimiehenkuja 4, 02150, Espoo, Finland

<sup>d</sup> School of Geography and Tourism, Shaanxi Normal University, 710119, Xi'an, China

<sup>e</sup> School of Resource, Environment and Earth Science, Yunnan University, 650500, Kunming, China

<sup>f</sup> TNO-Geological Survey of the Netherlands, Princetonlaan 6, 3584 CB, Utrecht, The Netherlands

### ARTICLE INFO

#### Article history:

Received 12 September 2017

Received in revised form

15 December 2017

Accepted 3 January 2018

Available online 12 January 2018

#### Keywords:

Provenance analysis

Sanmen Gorge

Mangshan Plateau

End member modelling

Grain-size

### ABSTRACT

The thick loess-palaeosol sequences in the Mangshan Loess Plateau (MLP; central China) along the south bank of the lower reach of the Yellow River provide high-resolution records of Quaternary climate change. In addition, substantial increases in grain-size and accumulation rate have been inferred in the upper part of the loess sequence, above palaeosol layer S2. This study investigates the sources of the long-term dust supply to the MLP and explores the mechanism behind the sudden increase in sediment delivery and coarsening of the loess deposits since S2 (~240 ka) by using end member modelling of the loess grain-size dataset and single-grain zircon U-Pb dating. Our results indicate that the lower Yellow River floodplain, directly north of the MLP, served as a major dust supply for the plateau at least since the deposition of loess unit L9 and indirectly suggest that the integration of the Yellow River and the disappearance of the Sanmen palaeolake took place before L9 (~900 ka). The sudden change in sedimentology of the Mangshan sequence above palaeosol unit S2 may result from an increased fluvial sediment flux being transported to the lower reaches of the Yellow River because of tectonic movements (initiated) in the Weihe Basin around 240 ka. Furthermore, sediment coarsening can be explained by the gradual southward migration of the lower Yellow River floodplain towards the MLP since the deposition of palaeosol S2. The migration is evidenced by the formation of an impressive scarp, and is likely caused by tectonic tilting of the floodplain area.

© 2018 Elsevier Ltd. All rights reserved.

### 1. Introduction

Quaternary loess-palaeosol sequences are widespread in the Chinese Loess Plateau (CLP) of northern China. The sedimentological characteristics of these wind-blown deposits provide a powerful tool for the reconstruction of the past atmospheric circulation pattern and climate change (Liu, 1985; Kukla, 1987; An

et al., 2001; Porter, 2001). A SE-ward decreasing trend in grain size, unit thickness and inferred sedimentation rate is recognised in the CLP loess sequences (Liu, 1985; Pye, 1995; Liu and Ding, 1998; Ding et al., 2002; Nugteren and Vandenberghe, 2004; Prins and Vriend, 2007). Two factors mainly control grain-size variations within the CLP, namely the strength of transporting winds and the locations of the source areas. Therefore, the sedimentary characteristics of the wind-blown deposits allow us to assemble information concerning past atmospheric circulation patterns and the distance to the source area. Previous studies suggested that the deserts and arid lands north and northwest of the CLP are the main source area of the CLP loess deposits (Liu, 1985; Derbyshire et al., 1998; Lu and Sun, 2000; Sun, 2003; Nugteren and Vandenberghe,

\* Corresponding author. Department of Geosciences and Geography, P.O. Box 64, 00014, University of Helsinki, Finland.

E-mail addresses: [yuan.shang@helsinki.fi](mailto:yuan.shang@helsinki.fi), [y.shang@vu.nl](mailto:y.shang@vu.nl) (Y. Shang).

<sup>1</sup> Present address: Department of Geosciences, UiT the Arctic University of Norway in Tromsø, Dramsveien 201, 9037 Tromsø, Norway.

2004; Ding et al., 2005). However, recent evidence based on single grain zircon U-Pb dating found a genetic link between the Yellow River and loess sediments. These results emphasise the important contribution of reworked fluvial detritus delivered by the Yellow River from the NE Tibetan Plateau to the CLP (Stevens et al., 2013; Bird et al., 2015; Nie et al., 2015; Licht et al., 2016; Zhang et al., 2016).

The Yellow River is the second longest river of China, with a total length of 5500 km. It originates in the northeast Tibetan Plateau and runs eastwards around the Ordos block and the North China Plain before discharging into the Bohai Sea (Fig. 1). The river course has traditionally been divided into upper, middle and lower reaches, with Hekou town in Inner Mongolia marking the upper/middle reach boundary, and Mengjin of Henan province the middle/lower reach boundary of the river (Fig. 1). As the most sediment-laden river in the world, the Yellow River delivered more than one billion tonnes sediments each year to the sea between

1951 and 1979 (Wang et al., 2015). Its sediment load increases most markedly in the middle reach, near the CLP and gradually declines downstream.

Geological surveying has identified a palaeolake in the Weihe Basin, with its eastern boundary at the Sanmen Gorge (AFSOM, 1988; Jiang et al., 2007). It has been suggested that the Sanmen palaeolake formed ~5 Ma (Wang, 2002) and was drained when the Yellow River started to cut the Sanmen Gorge, leading to the formation of its modern course (Jiang et al., 2007; Zheng et al., 2007; Wang et al., 2013). The proposed timing of the incision of the gorge varies from late Miocene to Pleistocene (Lin et al., 2001; Wang, 2002; Jiang et al., 2007; Wang et al., 2013; Kong et al., 2014; Hu et al., 2017), and Rits et al. (2017) concluded that the Sanmen Lake did not exist during the last ~1 Myr. The cutting of the Sanmen Gorge allowed the release and transport of substantial volumes of reworked loess towards the lower reaches of the river. As a result, large fluvial fan systems were created east of the Sanmen Gorge

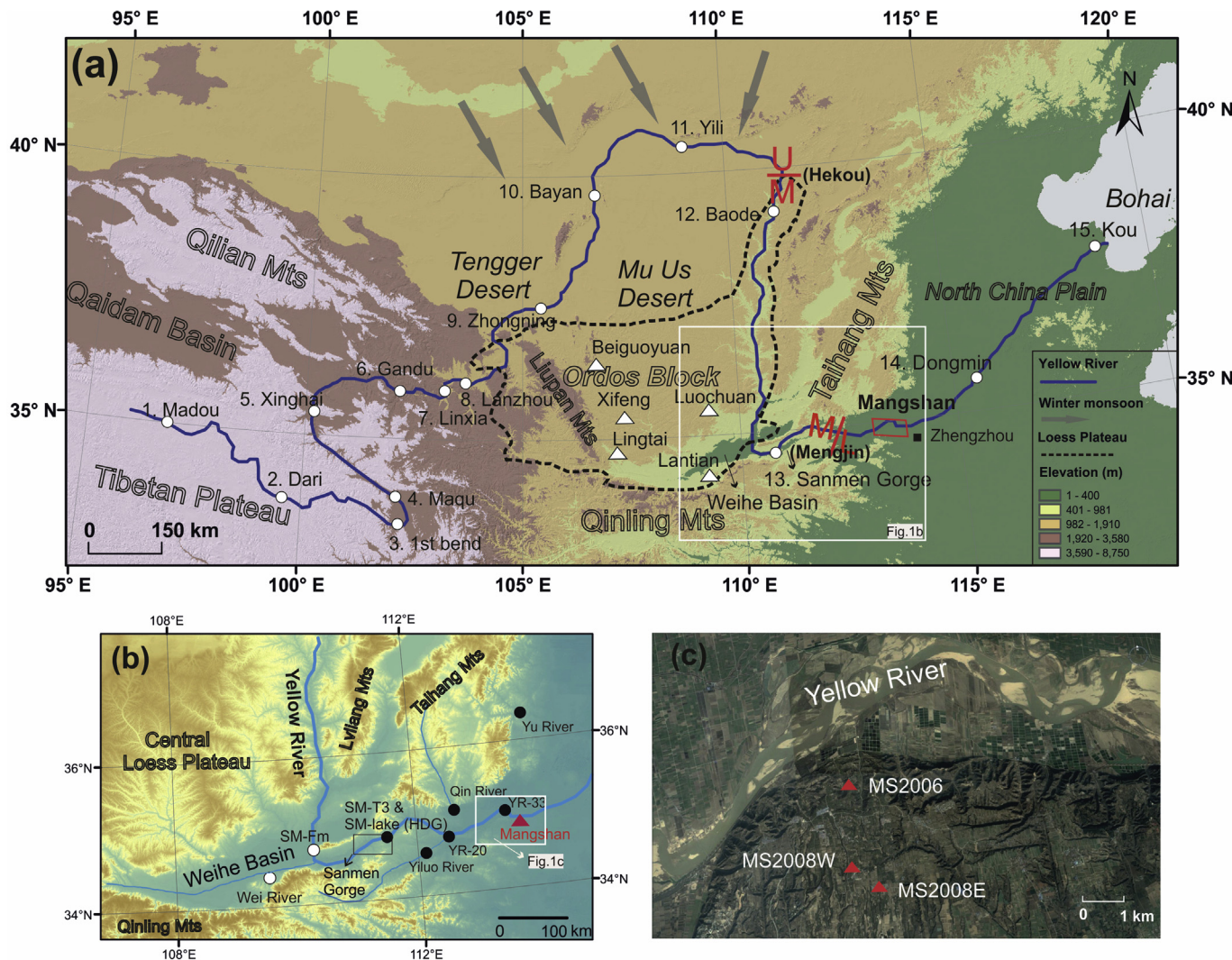


**Fig. 1.** (a) Digital elevation model (DEM) map of northern China showing the Yellow River, Chinese Loess Plateau (CLP) and Mangshan Loess Plateau (MLP). The grey arrows indicate the direction of winter monsoon winds. The red letters indicate the boundary of upper, middle and lower reaches of the Yellow River. The white dots indicate the previous published Yellow River samples of zircon U-Pb ages (Nie et al., 2015). Samples 1–11, 12–13 and 14–15 are representative for the upper, middle and lower reaches of the Yellow River respectively. (b) Map showing the zircon sampling sites in the Weihe Basin, middle and lower reaches of the Yellow River. The red triangle marks the MLP. The black dots show samples collected within this study while the white dots represent samples cited in Kong et al. (2014). Detailed sample description is presented in Table S3. HDG is abbreviation for Huangdigou, where SM-T3 and SM-lake being collected. (c) Loess section MS2006, MS2008W and MS2008E on the MLP of this study marked with red triangles. Figure (c) is produced with Google Earth Imagery © 2017 TerraMetrics. Data © Europa Technologies Ltd. (For interpretation of the references to colour in this figure legend, the reader is referred to the Web version of this article.)

(Huang et al., 2009). Studying the evolution of the Yellow River is crucial for understanding the “source-to sink” process, influenced by tectonic activity and climate change at both a regional and global scale. However, the geological history of the Yellow River remains a topic of debate and active investigation, particularly for the development of its drainage system in its middle and lower reaches (Lin et al., 2001; Wang, 2002; Jiang et al., 2007; Pan et al., 2011; Wang et al., 2013; Kong et al., 2014; Hu et al., 2017; Li et al., 2017).

Thick, continuous loess-palaeosol records of exclusively aeolian origin have been found on the Mangshan Loess Plateau (MLP) (Wu et al., 1999; Jiang et al., 2007; Zheng et al., 2007; Qiu and Zhou, 2015) which is located along the lower reach of the Yellow River (Fig. 1). Here the loess deposits above palaeosol S2 (equivalent to MIS 7, ca. 225 ka) are significantly thicker than loess deposits on the CLP. For instance, the deposits of L1-S1-L2 of Xifeng, Luochuan and Lantian are between 10 and 20 m thick, whilst those at Mangshan are ~86 m thick. Consequently, sedimentation rates and mass accumulation rates are significantly higher at the MLP than in the central CLP (Prins et al., 2009). In addition, the upper part of the Mangshan record displays extremely high sedimentation rates and a coarser composition compared to its lower part, suggesting a dust supply from a more proximal source, i.e. the lower Yellow River floodplain (Wu et al., 1999; Jiang et al., 2007; Zheng et al., 2007; Prins et al., 2009). Study of the provenance and sedimentological variations of the Mangshan loess records may therefore assist in the understanding of the mechanisms associated with dust supply from the Yellow River to the MLP and the drainage system development in the river's middle and lower reaches.

In this paper, the first record of single grain zircon U-Pb chronology of the Mangshan loess-palaeosol sequence is presented

(Figs. 2 and 5), from the Holocene soil S0 through L6 and L9) and is compared with the U-Pb age signature of possible sources, including the upper, middle and lower reaches of the Yellow River deposits, the CLP loess, as well as river sediments from the nearby Taihang Mountains and Qinling Mountains. By combining the provenance age distributions with a mixing model of the grain-size distribution data (Figs. 2 and 3) and a dust flux model (Fig. 4) of the Mangshan sequence(s), it is intended to 1) characterise the contribution of subpopulations of the sediments and their corresponding transporting processes based on the grain-size dataset, 2) investigate the provenance signal of the Mangshan loess, comparing it to potential source areas (Fig. 6) and quantify their contributions (Fig. 7), and 3) discuss the mechanisms controlling sedimentology and provenance variations of the Mangshan dust during the Pleistocene and Holocene. The results also have implications for the evolution of the Yellow River system and the age of the Sanmen palaeolake.

## 2. Material and methods

### 2.1. Sites, samples and sediment analyses

The MLP lies 25 km west of Zhengzhou on the south bank of the Yellow River (Fig. 1). The loess plateau is about 18 km in length (W-E) and 5 km in width (N-S), with its highest point reaching approximately 150 m above the Yellow River floodplain (Fig. S1). The deposits consist of a number of loess and palaeosol alternations with a total thickness of ~170 m (Jiang et al., 1998, 2004, 2007; Ji et al., 2004; Zheng et al., 2007). Zheng et al. (2007) showed that the upper part of the sequence (0–97 m, including palaeosols S0, S1

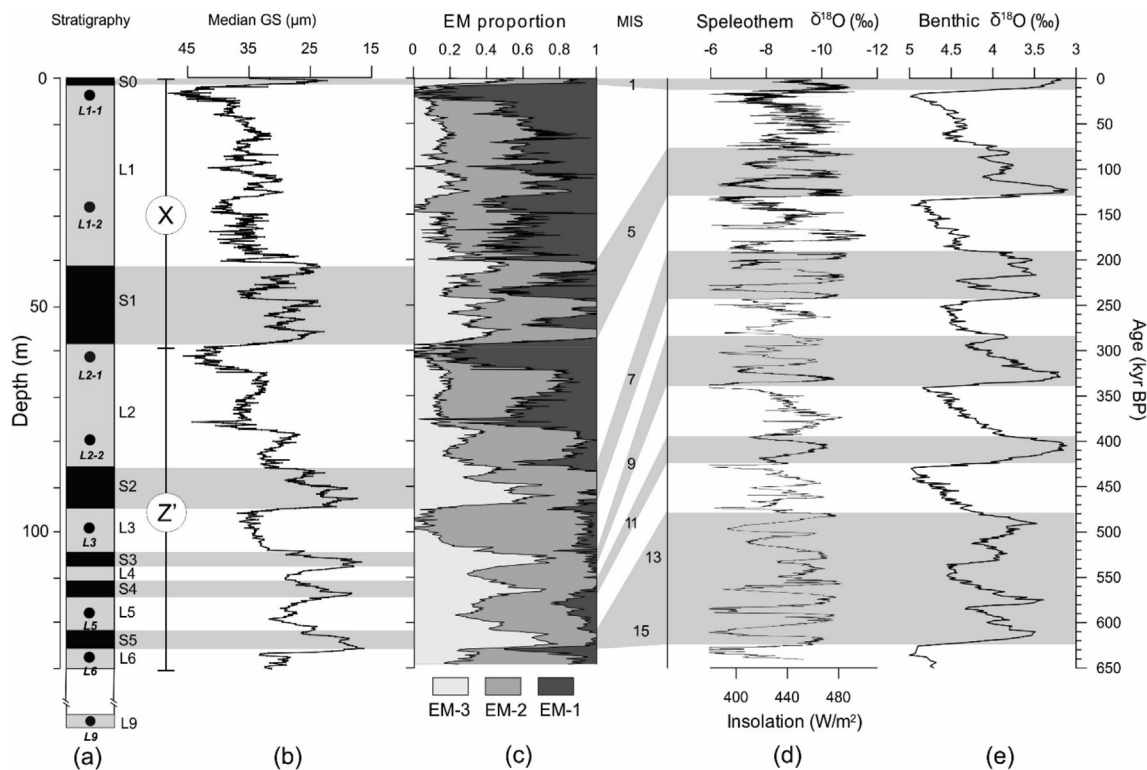


**Fig. 2.** (a) Palaeosol (S0, S1 … S5) and loess (L1, L2 … L6) stratigraphy in section MS2006 with black dots indicating the levels of zircon samples; (b) median grain size distribution of the MS2006 section, (c) the proportional contribution of the end members against depth. The age model of MS2006 is based on tuning to the following ‘target curves’ (time series): (d) the oxygen-isotope composite record from Dongge, Sanbao and Hulu caves in central China (Cheng et al., 2009, 2016; Wang et al., 2008), here superimposed on the summer (21 July) insolation at 65°N (Berger, 1978), and (e) the stacked marine benthic oxygen-isotope record (Lisicki and Raymo, 2005). The grey bars indicate palaeosol layers and corresponding interglacial stages/marine isotope stages (MIS). The tie points linking the loess-palaeosol record to the target isotope curves are listed in Table S1. Section MS2006 (a) is ~130 m thick and is a composite of record X (0–59 m; Prins et al., 2009) and record Z' (59–130 m; Zheng et al., 2007; see also Prins et al., 2009).

and S2, and loess units L1 and L2) experienced extremely high sedimentation rates (on average 40 cm/kyr) in comparison with the lower part of the profile (97–165 m; palaeosols S3–S10, loess units L3–L10) (see also Fig. S1).

Here the grain-size, magnetic susceptibility, carbonate content and organic matter records for the loess-palaeosol sequences are presented, based on samples from two localities (Fig. 1 and Figs. S1, S2 and S4). The northern ('proximal') loess section, here referred to as MS2006 (34°57.5' N, 113°22.2' E) (Fig. 1c), is exposed on the northern slope of the plateau, where the Yellow River and local gullies cut through the loess forming a valley with steep cliffs. Section MS2006 is ~130 m thick (Fig. S2) and is a composite of record X (0–59 m; Prins et al., 2009) and record Z' (36–130 m; Zheng et al., 2007; see also Prins et al., 2009), analysed at a 10-cm (X: 0–59 m) and 20-cm resolution (Z': 59–130 m). The grain-size, organic matter and carbonate profiles of records X and record Z' for the overlapping interval 36–59 m indicate the similarities between records X and Z' (Fig. S3). The uppermost S0-L1-S1 loess-palaeosol complex has also been sampled at a more southern location, about 2.0–2.7 km south of the MS2006 section (Fig. 1c and Figs. S1 and S4) to study the impact of increasing distance with respect to the Yellow River. The two sections MS2008W (34°56.4' N, 113°22.2' E) and MS2008E (34°56.1' N, 113°22.4' E), ~34 and ~14 m thick, respectively, have been sampled in 26 partly-overlapping vertical trenches at a 10-cm resolution.

## 2.2. Magnetic susceptibility, carbonate and organic matter analysis

The samples were dried in an oven (50 °C), lightly ground and aliquots of ~8 g were analysed using a Bartington MS2 magnetic susceptibility meter at the School of Ocean and Earth Sciences, Tongji University (Shanghai). The organic matter and carbonate content of aliquots of ~2 g of these samples were analysed by thermo-gravimetric analysis (TGA), using a Leco TGA 601 at the Vrije Universiteit Amsterdam (VUA). Derivative weight loss curves most clearly indicate the temperature intervals during which weight loss is most apparent: replicate tests performed on the loess samples indicate that the temperature interval during which organic matter and carbonate minerals disintegrate is from 200 to 550 °C and 700–1000 °C, respectively.

## 2.3. Grain-size analysis and end-member modelling

The Mangshan loess samples for grain-size analysis were prepared following the methods described by Konert and Vandenberghe (1997), with organic matter and carbonates being removed. All the measurements were performed on a Fritsch Analysette 22 laser particle sizer at the VUA resulting in a grain-size distribution with 56 size classes in the size range 0.15–2000 µm.

A mixing model of the combined Mangshan grain-size distribution dataset ( $n = 1931$ , from sections MS2006, MS2008W and 2008E) was constructed with the inversion algorithm for end-member modelling of compositional data EMMA (Weltje, 1997). EMMA is a non-parametric numerical-statistical technique and its advantage over the parametric curve fitting approaches, e.g. Weibull (Sun et al., 2002, 2004) or log-normal (Xiao et al., 2009, 2013) is that it does not require any prior knowledge about the grain size controlling processes (Weltje and Prins, 2007). This method has proven to be powerful in distinguishing aeolian from fluvial sediments in various marine settings (e.g. Prins and Weltje, 1999; Prins et al., 2000; Stuut et al., 2002, 2014; Deplazes et al., 2014) and in partitioning multiple transport/deposition processes of Quaternary loess from the CLP (Prins and Vriend, 2007; Prins et al., 2007; Vriend et al., 2011; Shang et al., 2017). Details of the technical aspects of the end-member modelling algorithm are given in Weltje

(1997), Prins and Weltje (1999) and Weltje and Prins (2003). Prins et al. (2009) already applied this approach to the grain-size data of the upper 60 m of the MS2006 section (Fig. 3d). In this study, a new mixing model expressing the loess samples from all three sections as mixtures of three end members has been produced.

The EMMA approach involves two modelling stages. In the first stage, the number of end members (EMs) is estimated on the basis of the mean and/or median coefficient of determination statistics ( $r^2$ , Fig. 3a). The coefficients of determination represent the proportions of the variance of each variable (size class) that can be reproduced by the approximated data (Fig. 3b). In principle, the simplest model is chosen when the  $r^2$  shows satisfactory goodness of fit (usually  $r^2 > 0.8$ , e.g. Fig. 3a). In the second modelling stage, the compositions of the end members are estimated (Fig. 3c) and the proportional contributions of the end members in the analysed samples are calculated (Fig. 2c).

## 2.4. Age model and dust flux calculations

Peterse et al. (2011) presented an age model for the upper 0–60 m (S0-L1-S1) of the sequence in section MS2006, and sections MS2008W and MS2008E based on the correlation of the typical loess proxy records, i.e. magnetic susceptibility, carbonate content and grain size, with the U-<sup>230</sup>Th dated oxygen isotope records from Dongge, Sanbao and Hulu caves in central China (Cheng et al., 2009; Wang et al., 2008). Following a similar approach, we extended the age model for the upper 130 m (S0-L6) of the loess-palaeosol sequence MS2006 (Fig. 2a, b, c) based on the correlation of loess proxy records with the newly published speleothem records extended to 640 kyr B.P. in central China (Fig. 2d; Cheng et al., 2016, and references therein). The inflection points in the loess proxy records have been used as tie points between the loess record and the MIS boundaries recognised in the stacked speleothem  $\delta^{18}\text{O}$  record. The depth and ages of the 11 selected time control points are listed in Table S1. Simultaneously, the loess-palaeosol sequence was also visually correlated with the stacked benthic oxygen isotope record (Lisiecki and Raymo, 2005) assuming that the palaeosols layers (S0, S1 … S5) correlate to interglacial Marine Isotope Stages (MIS1, 5 … 13–15) and the loess layers (L1, L2 … L5) correlate to glacial Marine Isotope Stages (MIS 2–4, 6 … 12) (Fig. 2e). Although a fully independent age control for the complete studied sequence is missing, a recent study by Qiu and Zhou (2015) provided OSL ages for the upper ~120 m of another section (covering the S0 to S5 interval) on the Mangshan Plateau. Their independent age model (based on the application of an elevated temperature post-IR IRSL (pIR<sub>200</sub>IR<sub>290</sub>) SAR procedure to polymimetal fraction) is very similar to our findings presented in Fig. 4 indicating that our age model suffices for the purpose of dust flux calculations.

Mass-accumulation rates (MAR, in g/cm<sup>2</sup>/ka) of the well-constrained loess (L1, L2 … L5) and palaeosol (S0, S1 … S5) units of sections MS2006 and MS2008W were calculated according to Prins and Vriend (2007):

$$\text{MAR} = \text{SR} \times \text{BD} \quad (1)$$

Where SR is the sediment accumulation rate (in cm/ky), and BD is the sediment dry-bulk density (in g/cm<sup>3</sup>). SR values were calculated based on the age estimates (Table S1) and sediment thickness values for each of the loess and palaeosol intervals (Table S2). BD values of 1.48 g/cm<sup>3</sup> were used (cf. Kohfeld and Harrison, 2003).

Fractionated mass-accumulation rates (fluxes) for the modelled end members ( $F_{\text{EM}-x}$ , in g/cm<sup>2</sup>/ka) were calculated according to Prins and Vriend (2007):

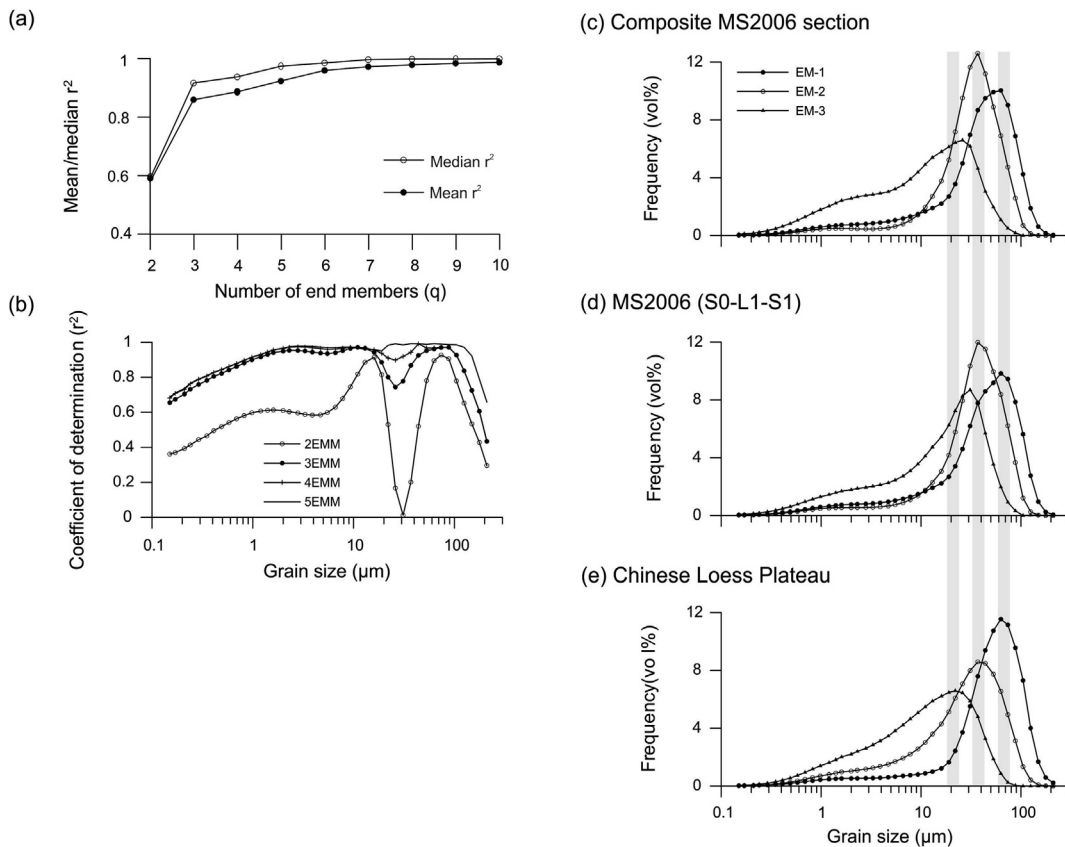


**Fig. 3.** End-member modelling results of the composite MS2006 section. (a) The mean/median  $r^2$  across the full-size range as a function of the number of end members ( $q$ ). (b) Coefficient of determination ( $r^2$ ) statistics for each size class for end-member models (EMM) with 2–5 end members. (c) Modelled end members according to a three-end-member model representing sandy loess (EM-1, modal size ~63  $\mu\text{m}$ ), silty loess (EM-2, modal size ~37  $\mu\text{m}$ ) and clayey loess (EM-3, modal size ~26  $\mu\text{m}$ ) for the composite MS2006 section in this study, (d) the last glacial-interglacial sequence (S0-L1-S1) from the Mangshan Plateau (Prins et al., 2009) and (e) the Chinese Loess Plateau (Prins and Vriend, 2007).

$$F_{\text{EM}-x} = \text{MAR} \times p_{\text{EM}-x} \quad (2)$$

Where  $p_{\text{EM}-x}$  is the proportional contribution (dimensionless) of end member EM- $x$ , and  $\sum_{x=\text{EM}-1}^{\text{EM}-3} p_x = 1$ .

In these calculations it was assumed that the loess-palaeosol samples are entirely composed of siliciclastics, which is just a first-order approximation as the contribution of other (non-siliciclastic) sediment phases like (detrital, pedogenic) carbonates and organic carbon has been ignored.

## 2.5. Zircon samples and zircon U-Pb dating

The zircon samples were collected from the MS2006 section, from loess units L1, L2, L3, L5, L6 and L9 (as a reference sample for the bottom loess unit, Figs. 2 and 5). Samples collected from potential source areas in this study are shown in Fig. 1b, including fluvial samples from the lower Yellow River, Yiluo River, Qin River and the Yu River alluvial fan northeast to the MLP. The detailed location and description of zircon samples including those from Kong et al. (2014), Bird et al. (2015) and Nie et al. (2015) are shown in Table S3.

The zircon grains in the size range of 20  $\mu\text{m}$ –90  $\mu\text{m}$  were extracted following the standard procedure of heavy liquids and Frantz magnetic separation at the Mineral Separation Laboratory of VUA (Shang et al., 2016) and randomly selected by hand-picking under an optical microscope and then mounted in epoxy resin and sectioned approximately in half and polished. Back-scattered electron images (BSE) were prepared for the zircons to target the

spot sites. U–Pb dating analyses were performed using a Nu Plasma AttoM single collector ICPMS connected to a Photon Machine Excite laser ablation system at the Geological Survey of Finland in Espoo. Typical ablation conditions were: beam diameter: 20  $\mu\text{m}$ , pulse frequency: 5 Hz, beam energy density: 2 J/cm<sup>2</sup>. Raw data were corrected for the background, laser induced elemental fractionation, mass discrimination and drift in ion counter gains and reduced to U–Pb isotope ratios by calibration to concordant reference zircons, using the program Glitter (Van Achterbergh et al., 2001). Age related common lead (Stacey and Kramers, 1975) correction was used when the analysis showed common lead contents significantly above the detection limit (i.e., >50 cps). All the ages were calculated with  $2\sigma$  errors and without decay constants errors.  $^{206}\text{U}/^{238}\text{Pb}$  and  $^{207}\text{Pb}/^{206}\text{Pb}$  ages were used for ages younger and older than 1 Ga, respectively. We used a 10–20% discordance filter to the generated data.

## 3. Results

### 3.1. Mangshan loess-palaeosol stratigraphy and sedimentology

The carbonate, organic matter and median grain-size records of section MS2006 are shown in Fig. S2. On the basis of these parameters a clear distinction can be made between the loess and palaeosol layers. Palaeosol layers S0 to S5 characteristically consist of fine-grained sediments, i.e. median grain-size values below 25  $\mu\text{m}$ , with low carbonate contents (1–2%) and slightly, but consistently, elevated organic matter contents (up to 1.5–2%). In

contrast, loess layers L1 to L6 consist of coarser sediments, with median grain-size values up to 30–35  $\mu\text{m}$  in the lower part of the sequence (L3–L6), and up to ~45  $\mu\text{m}$  in loess horizons L2 and L1. The loess sediments typically show carbonate contents of ~10%, and low organic matter values (~0.5–0.75%). Distinct layers with high carbonate content (>10%) – reflecting the presence of carbonate nodules – occur near the base of palaeosol layers S1, S2, S3 and S4.

A detailed stratigraphic picture of the S0-L1-S1 sequence in section MS2006, and its correlation with sections MS2008W and MS2008E, is shown in Fig. S4. Overall, the three sections show relatively consistent trends in the analysed proxies during the last glacial-interglacial cycle: glacial loess unit L1 is characterised by relatively lower magnetic susceptibility of ~5 SI/g, higher carbonate content of ~10% and a coarser median grain size (30–50  $\mu\text{m}$ ), while a higher magnetic susceptibility (5–10 SI/g), lower carbonate content (<10%) and finer median grain sizes (20–40  $\mu\text{m}$ ) characterise the interglacial palaeosol units S1 and S0. In addition, higher-frequency and lower-amplitude patterns are visible in all three proxy records, within palaeosol unit S1 and especially in the loess unit L1, pointing to highly variable sedimentation and pedogenic processes throughout the last glacial-interglacial cycle. The thickness of the loess unit L1 and palaeosol unit S1 decreases from the northern MS2006 section to the southern MS2008W and MS2008E sections (Figs. S1 and S4). For example, the thickness of L1 of the MS2006 section is about 42 m while in the MS2008W, it is around 22 m.

### 3.2. Mixing model

The ‘goodness-of-fit’ ( $r^2$ ) statistics were computed for mixing models with 2–10 end members. The results show that the loess sediments can be adequately described as mixtures of three end members (Fig. 3a and b). The three-end-member model explains on average more than 86% of the observed variance in the grain-size dataset (mean  $r^2$  of 0.86 and a median  $r^2$  of 0.92, Fig. 3b).

The end members are characterised by unimodal, fine skewed grain-size distributions (Fig. 3c) with modal particle sizes close to 63  $\mu\text{m}$  (EM-1), 37  $\mu\text{m}$  (EM-2) and 26  $\mu\text{m}$  (EM-3). The sand (>63  $\mu\text{m}$ ): silt (8–63  $\mu\text{m}$ ): clay (<8  $\mu\text{m}$ , cf. Konert and Vandenberghe, 1997) ratio for EM1, EM2 and EM3 are 32:54:14,

15:76:9 and 2:55:43, respectively. The modelled end members presented here for the complete Mangshan dataset (Fig. 3c) resemble those of the upper (S0-L1-S1) Mangshan sequence (Fig. 3d) presented by Prins et al. (2009) and the CLP loess dataset (Fig. 3e) presented by Prins and Vriend (2007).

The proportional contribution of the end members with depth in the MS2006 section is compared to the loess-palaeosol stratigraphy and median grain-size record in Fig. 2. An evidently dramatic increase of the sandy EM-1 in the loess units and palaeosol units above S2 is present. By contrast, the proportion of clayey EM-3 decreased in the palaeosol units S0 and S1 compared to the lower units S2, S3, S4 and S5 (Fig. 2c).

A detailed picture of the S0-L1-S1 sequence in sections MS2006, MS2008W and MS2008E is depicted in Fig. S5. The proportion of the sandy EM-1 in MS2006 is significantly higher than in the southern two sections MS2008W and MS2008E which are situated at a more distant location with respect to the Yellow River floodplain (Fig. 1c and Fig. S1), whereas the proportions of the silty EM-2 increase from the northern MS2006 section to MS2008W and MS2008E (Fig. S5). The clayey EM-3 does not show a clear spatial increasing/decreasing trend. These trends suggest that the sandy and silty end-members of the upper three units (S0-L1-S1) of the Mangshan loess were derived from a nearby source area, the lower Yellow River floodplain, see below in the Discussion.

### 3.3. Dust flux model

Linear sediment accumulation rate (LSR), mass accumulation rates (MAR) and fractionated fluxes of the three end-members (FEM-1, FEM-2 and FEM-3) were calculated for the stratigraphic units of section MS2006 (S0-L1-S1 … L5-S5) and MS2008W (S0-L1-S1). Overall, a dramatic increase in the LSR is observed in the upper part of MS2006 section (above S2) (Fig. 4a). The average SR value for the upper part of MS2006 section is 36 cm/kyr while for the lower part (below S2) it is about 11 cm/kyr. In more detail, the SR record shows an increasing trend from the base (S5) to the top (L1), superimposed on a clear glacial-interglacial variability with high LSR recorded during glacials (loess units) and low LSR during interglacials (palaeosol units).

Fig. 4b shows that bulk MAR values range between ~4 and ~88 g/

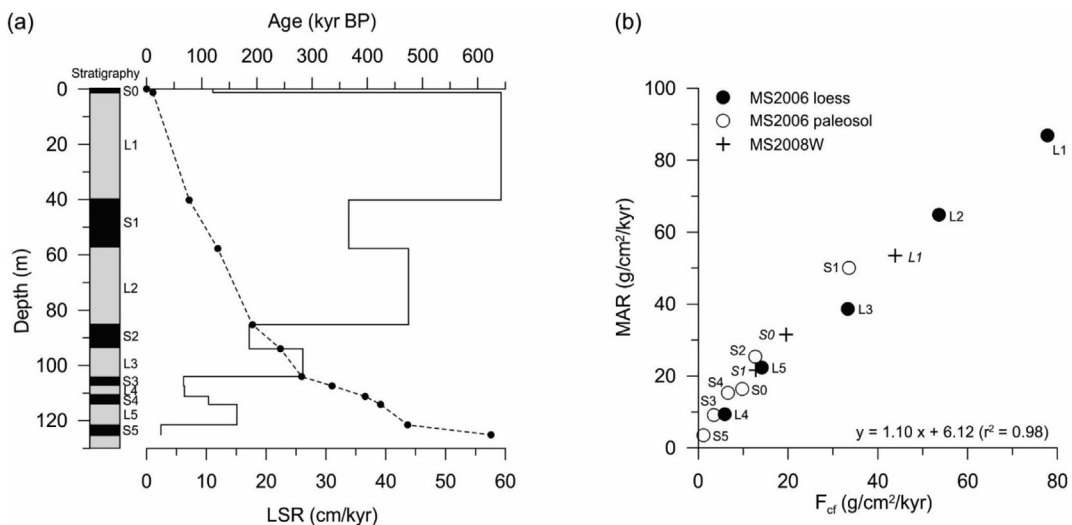


**Fig. 4.** (a) Age-depth plot (dashed line) of the loess-palaeosol boundaries in the MS2006 section, based on the correlation of the loess-palaeosol record to the target isotope curves shown in Fig. 2, and corresponding linear sedimentation rate (LSR) estimates per loess and palaeosol unit (solid line). (b) Scatter plot of the ‘coarse fraction’ flux ( $F_{cf}$ , i.e. flux of EM1 and EM2) versus the total mass-accumulation rate (MAR) of all major loess (L1, L2 … L5) and palaeosol units (S1, S2 … S5) in MS2006 (and MS2008W, see legend). Linear regression formula for the MS2006 data set is shown. Data are listed in Table S1 and Table S2.

$\text{cm}^2/\text{kyr}$  in section MS2006, with minimum values in the S5 palaeosol unit and maximum values in the L1 loess unit. The MAR values in section MS2008W varied between  $\sim 22$  and  $\sim 53 \text{ g/cm}^2/\text{kyr}$ , with minimum values in the S1 palaeosol unit and maximum values in the L1 loess unit. Similar to the SR record, the loess units display higher MAR than the palaeosol units. However, there is a significant increase in MAR from S2 and above. Note that the MAR values in palaeosol units S2 ( $25 \text{ g/cm}^2/\text{kyr}$ ) and S1 ( $50 \text{ g/cm}^2/\text{kyr}$ ) are even higher than the pure loess units L4 ( $9 \text{ g/cm}^2/\text{kyr}$ ) and L5 ( $22 \text{ g/cm}^2/\text{kyr}$ ). Spatially, the loess unit L1 and palaeosol unit S1 of the MS2006 section also display overall higher MAR values compared to the units of MS2008W section, which is at a greater distance from the Yellow River.

The summed fractionated fluxes of the coarse fraction ( $F_{\text{cf}} = F_{\text{EM-1}} + F_{\text{EM-2}}$ ) are plotted against the bulk MARs of the stratigraphic units in the sections MS2006 and MS2008W in Fig. 4b. The coarse fraction and MAR are positively related by the linear regression equation:  $\text{MAR} = 1.10F_{\text{cf}} + 6.12$  ( $r^2 = 0.98$ ). “6.12” reflects the constant absolute contribution of EM-3 over time. The variations in relative EM-3 content are thus dominantly caused by a variable input of end-members EM-1 and EM-2, with a negative relation between EM-3 and MAR. Similar results have been described by Prins and Vriend (2007), Prins et al. (2007) and Vriend et al. (2011) from the CLP.

### 3.4. The zircon U-Pb age distributions

#### 3.4.1. Mangshan loess-palaeosol sequence

Fig. 5 displays the zircon U-Pb age distributions for the Mangshan loess samples next to the loess-palaeosol stratigraphy. All the loess samples are characterised by two dominant age populations, one at 200–350 Ma (Permian–Triassic population) and the other at 350–550 Ma (Ordovician–Silurian population). Additionally, there are several minor age peaks in the ranges of 0–100 Ma, 0.7–1 Ga, 1.5–2.0 Ga and at ca. 2.5 Ga. However, the relative abundance of the two dominant age peaks (200–350 Ma and 350–550 Ma) varies from sample to sample. The abundance is almost equal for the samples from the loess units L1 (MS-L1-1 and MS-L1-2) and L3 (MS-L3) whereas the age population at 200–350 Ma is more notable in sample MS-L2-1 from the upper part of loess unit L2, and the peak at 350–550 Ma is dominant in the samples from the lower part of L2 (L2-2), the loess units L5 (MS-L5), L6 (MS-L6) and L9 (MS-L9).

In order to minimise uncertainty introduced by varying number of grains analysed for each sample ( $n = 213$ –347), and to make the results more statistically meaningful, the zircon ages were grouped into an upper and a lower Mangshan section. The comparison of the combined age spectra above S2 ( $n = 1100$ ) to those below S2 ( $n = 903$ ) shows that the age populations 200–350 Ma and 350–550 Ma are dominant in both datasets (Fig. 6a and b), although, the <100 Ma and the 200–350 Ma age populations slightly increase (compared to the 350–550 Ma population) in the upper part of the Mangshan sequence.

#### 3.4.2. Comparison of Mangshan loess with potential source areas

Grain-size analyses and end-member modelling indicated that the nearby lower Yellow River floodplain is the likely source of the sandy and silty loess components. The comparison of the zircon U-Pb age spectra of the Mangshan loess with potential source areas (Fig. 6) confirm this and indicate that the overall pattern of Mangshan zircon U-Pb ages (Figs. 6a and b) is not only comparable to that of the lower reaches of the Yellow River as sampled at locations YR-20 and YR-33 (Fig. 1b; Figs. 6k and l) but also to that of the loess deposits from the CLP (Beiguoyuan and Lingtai, Fig. 1; Fig. 6c), and even the upper reaches of the Yellow River (Fig. 6m). All these

deposits exhibit two distinct Palaeozoic age populations at 200–350 Ma and 350–550 Ma (Figs. 6k, l and o). Additionally, the upper part of Mangshan loess record shows a <100 Ma zircon age peak (Fig. 6a). The zircon ages of the Mangshan loess are different from those of the middle reach of the Yellow River (Fig. 6n), which are characterized by only one dominant Palaeozoic age peak at 200–350 Ma and two old zircon populations at ca. 1850 Ma and ca. 2500 Ma (Stevens et al., 2013; Bird et al., 2015; Nie et al., 2015). The Qin River and Yu River alluvial fan zircon ages (Figs. 6i and j), considered to be representative of the provenance signal from the Taihang Mountains (Figs. 1a and b), are dominated by older zircon grains with age peaks at ca. 1850 Ma and ca. 2500 Ma, respectively. The Yiluo River sample – representing the Qinling Mountains source (Figs. 1a and b) – displays similar double-age peaks at 200–350 Ma and 350–550 Ma (Fig. 6d) as the Mangshan loess samples, with an additional younger age peak in the range of 60–180 Ma and a distinct peak at ca. 2300 Ma, not present in the Mangshan loess. The Wei River, with its course north of the Qinling Mountains (Fig. 1b), forms an important tributary of the Yellow River and carries sediments that are dominated by the 200–300 Ma and especially the 350–550 Ma age populations (Fig. 6e). Notably, zircon grains of early Cenozoic age (0–60 Ma) are also present in the Wei River sediments. Zircon ages of sediments from the Sanmen Gorge (Figs. 1a and b), including Sanmen palaeolake sediments (Fig. 6h), fluvial sands of the Sanmen Formation (Fig. 6f) and from the third and oldest river terrace (T3) of the Yellow River in Huangdigou (HDG) of the Sanmen Gorge (Fig. 6g) (Wu et al., 1999) – all exhibit dominant peaks corresponding to 200–350 Ma and 350–550 Ma, with two minor peaks at ca. 1850 Ma and ca. 2500 Ma.

Non-metric Multi-Dimensional Scaling (MDS) maps (Vermeesch, 2013; Vermeesch et al., 2016) are used to visualize the (dis-) similarities between the zircon age profiles of Mangshan loess, CLP loess, Yellow River sediments and other potential contributors to the Mangshan loess (Fig. 7). The Mangshan loess plots close to the samples from the upper reach of the Yellow River and the CLP loess. The samples from the lower reach of the Yellow River shows a close link with both the Wei River and the Yiluo River samples. The samples of the Sanmen palaeolake and the river terraces in the Sanmen Gorge are located very close to each other. The Qin River sample and the Yellow River middle reach sample lie close to each other but plot away from other samples in the map.

## 4. Discussion

### 4.1. Genetic interpretation of the Mangshan loess end-member model

The end-member modelling results of the Mangshan loess-palaeosol grain-size record show that the sediments are well described as a mixture of three different dust components which are comparable to the average mixing model of the CLP (Figs. 3c and e) (Prins et al., 2007; Prins and Vriend, 2007). Prins et al. (2007) interpreted the CLP loess-palaeosol records contain two different types of aeolian dust supplied from two distinct source areas and/or reflecting different sediment transport-deposition process. The sandy (EM-1) and silty (EM-2) loess components represent the coarse dust fraction transported by low level continental northwesterly monsoonal winds via modified saltation and short term suspension processes over relative short transport distances during major dust outbreaks. By contrast, the clayey loess component (EM-3) reflects a fine dust component distributed over longer distances by long-term suspension processes. The fact that EM-1 and EM-2 are dominant in the Mangshan sequences indicates that most of the Mangshan loess was supplied from a proximal source during major dust events. The independent mixing model of the last

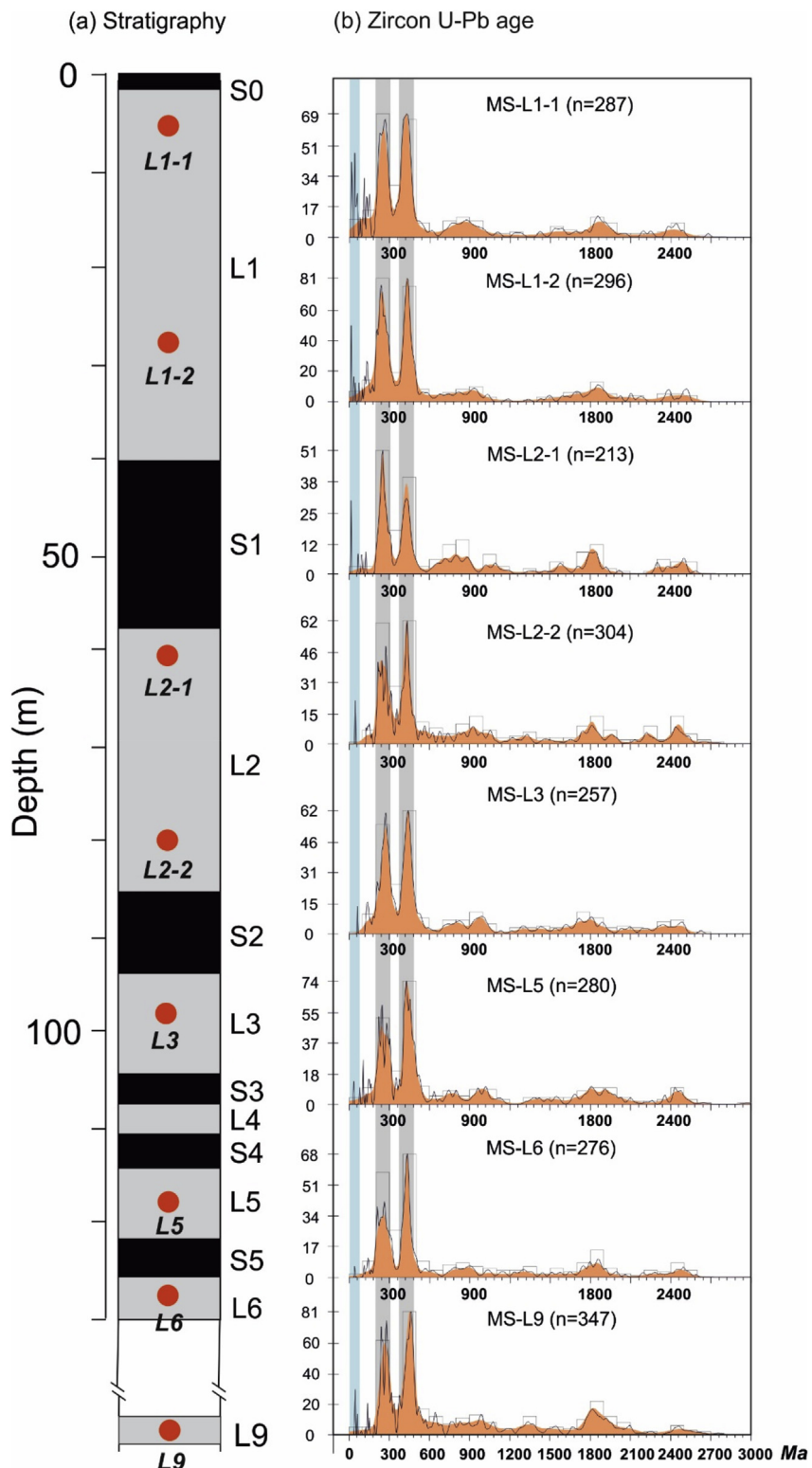


**Fig. 5.** (a) Palaeosol (S0, S1 … S5) and loess (L1, L2 … L6) stratigraphy in section MS2006 with red dots showing the level of samples for zircon U-Pb age analysis. (b) Zircon U-Pb age distributions of Mangshan loess samples. The black lines are normalised probability density function plots (PDF); the orange shades are Kernel Density Estimation (KDE) plots for different units; the open rectangles are age histograms. The blue rectangle indicates the 0–100 Ma age population while grey rectangles mark the dominant age population 250–350 and 350–550 Ma in the spectra. (For interpretation of the references to colour in this figure legend, the reader is referred to the Web version of this article.)

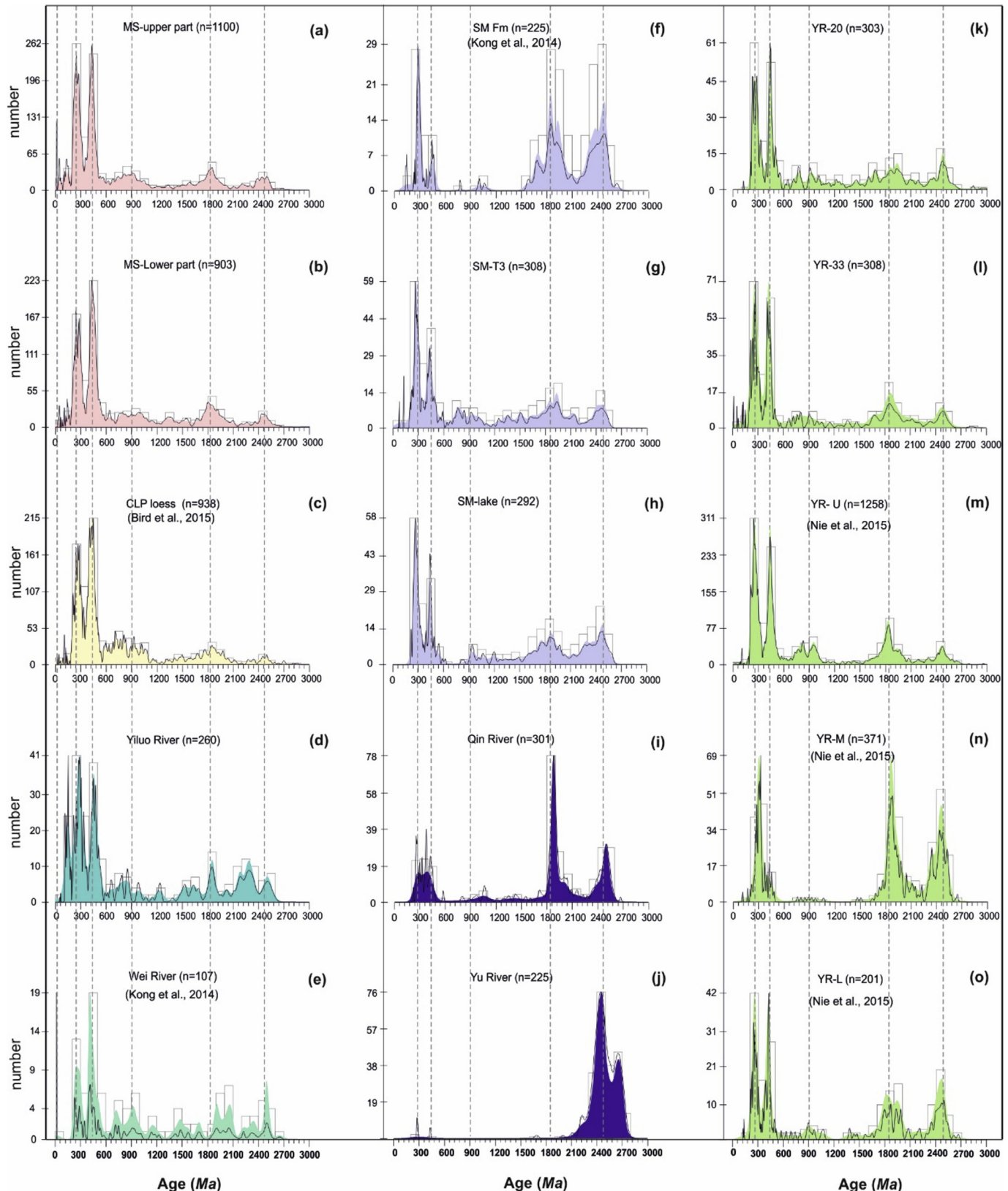


**Fig. 6.** Detrital zircon U-Pb ages for samples analysed within this study and the previously published dataset for CLP loess (Bird et al., 2015), the Wei River (Kong et al., 2014), the Sanmen Formation (Kong et al., 2014) and the Yellow River upper, middle and lower reaches (Nie et al., 2015). The samples' locations are indicated in Fig. 1 and detailed description are presented in Supplementary Table S3. MS-upper (6a) and MS-lower (6b) are the combined zircon age dataset of samples from the upper part (L1-1, L1-2, L2-1 and L2-2) and lower part (L5, L6 and L9) of the MS2006 section respectively. Note we excluded sample L3 from the combination dataset because loess unit L3 is a transition period in the sedimentology of the stratigraphy. The black lines are normalised probability density function plots (PPD); the colour shades are Kernel Density Estimation (KDE) plots for different units and the open rectangles are age histograms. Vertical dash lines indicate the major age peaks of the spectra.

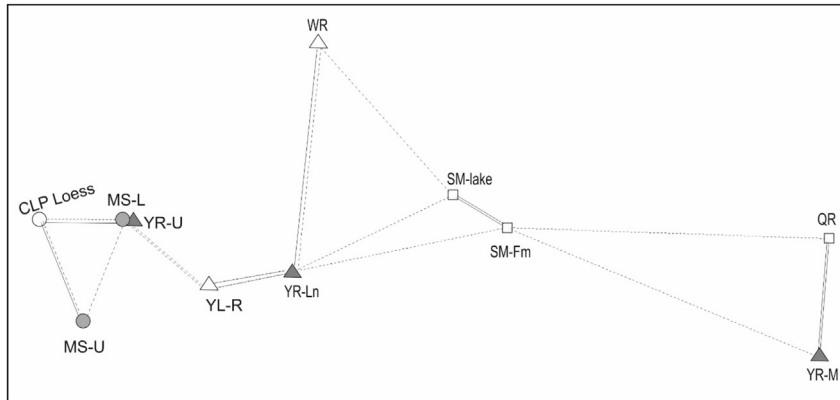


**Fig. 7.** Non-metric multi-dimensional scaling (MDS) map visualising the comparison between the Mangshan zircon age dataset (MS-U and MS-L), the loess of the Chinese Loess Plateau (CLP Loess), and zircon datasets of fluvial deposits of the Yellow River upper reach (YR-U), middle reach (YR-M) and lower reach (YR-Ln), combination dataset of samples YR-L, YR-20 and YR-33 in Fig. 6), the Yiluo River (YL-R), the Wei River (WR), the Qin River (QR) and samples of the Sanmen palaeolake (SM-lake) and fluvial sands of the Sanmen Formation (SM-Fm). The stress value is 0.35%, indicating an “excellent fit” of the data. The solid lines link the closest neighbours and the dashed lines the second closest neighbours.

glacial-interglacial sequence (S0-L1-S1) of the MS2006 section (Prins et al., 2009) shows that the clayey or ‘fine silty’ EM3 of the upper Mangshan sequence (with the mode at 32  $\mu\text{m}$ ; Fig. 3d) is coarser than EM3 of the composite MS2006 section (mode at 26  $\mu\text{m}$ ; Fig. 3c). This observation suggests that the new mixing model allows better to make the distinction between the two types of dust supply patterns also observed on the CLP.

According to the equation  $\text{MAR} = 1.10F_{\text{cf}} + 6.12$  ( $F_{\text{cf}} = F_{\text{EM-1}} + F_{\text{EM-2}}$ ) (section 3.3), the variation of  $F_{\text{EM-3}}$  can be explained as a result of a “dilution effect” from the variation of the coarse flux  $F_{\text{EM-1}}$  and  $F_{\text{EM-2}}$ , with high EM-3 content reflecting low MARs and low EM-3 content reflecting high MARs. Thus, variations in dust flux during glacials and interglacials are expressed by relative high EM-3 content in palaeosol units (S1, S2, S3, S4 and S5) and lower relative EM-3 content in loess units (L1, L2, L3, L4 and L5, Fig. 2c). The relative content of fine EM-3 in loess units L1, L2 and L3 in the MS2006 section is significantly lower than in the loess units L4, L5 and L6 in the lower part of the sequence, because of a higher input of the coarse dust fraction of EM-1 and EM-2 ( $F_{\text{EM-1}} + F_{\text{EM-2}}$ ) in the loess units L1, L2 and L3, particularly in L1 and L2. This is due to a dramatically increased dust accumulation rate in the MS2006 section since the deposition of L3 (243–280 ka). It is noticeable that both median grain size and proportions of modelled end members of the Mangshan record fluctuate more frequently in the loess units L1 and L2 and palaeosol unit S1 (Fig. 2). This observation might reflect more variable climatic conditions during the last two glacial-interglacial cycles.

The results show a downwind (N-S) thinning and fining trend in grain-size (Fig. S5). In addition, the proportion of modelled coarse fraction EM-1 also decreases from the MS2006 section to the more distal MS2008W and MS2008E (Fig. S1). This spatial grain-size and EM-1 distribution pattern is also observed over a much larger scale across the CLP (Prins et al., 2007; Prins and Vriend, 2007). Although this N-S downwind pattern here is observed over a relatively small spatial scale (2.0–2.7 km), it likely suggests a proximal source region to the north of the MLP, i.e. the Yellow River floodplain for the Mangshan loess deposits, and indicates that the near-surface northwesterly/northerly winter monsoon winds are responsible for the transportation of the dust from the source area to the Mangshan Plateau.

#### 4.2. Provenance signals of the Mangshan loess sequences

The overall zircon age distributions (Fig. 6) and the MDS map

(Fig. 7) show that the Mangshan loess deposits resemble those of the sediments from the upper and lower reaches of the Yellow River and of the CLP loess. A genetic link between Yellow River sediments and CLP loess has already been proposed in previous studies (Stevens et al., 2013; Bird et al., 2015; Nie et al., 2015). These studies suggested that the deposits on the CLP are largely derived from the northeastern Tibetan Plateau (NTP) carried by the Yellow River and later reworked by aeolian processes. A recent study by Licht et al. (2016) indicated further that the reworked Yellow River sediments account for 60–70% of the supply to the CLP dust. The end member modelling on the grain-size distribution of the Mangshan loess deposits imply that the coarse dust fractions EM1 and EM2 are derived from the Yellow River floodplain just north of the MLP. Together with the zircon U-Pb age spectra this seems to indicate that the Mangshan loess deposits have been constantly supplied by the lower Yellow River floodplain since L9.

Sediments of the upper reach of the Yellow River exhibit two distinct Palaeozoic zircon age populations at 200–350 Ma and 350–550 Ma matching the NTP provenance signatures. The lower reach of the Yellow River, after the confluence of Wei River and Yiluo River, shows a similar zircon age distribution as the upper reach of the Yellow River (Figs. 6m and o). According to Nie et al. (2015), this indicates the effects of the Wei River and the Yiluo River (Fig. 1b) which have brought abundant Phanerozoic zircon grains with a double peak (200–550 Ma) from the Weihe Basin and Qinling Mountains to the lower Yellow River (Fig. 6), resulting in a similar signal between the lower and upper reaches despite different source admixtures. In contrast, the sediments of the middle reach of the Yellow River are distinctive from the upper and lower reaches of the river by displaying a prominent single peak Palaeozoic age population at ca. 300 Ma (Fig. 6n) and two old Proterozoic age populations at ca. 1850 Ma and ca. 2500 Ma. These ages are more similar to the source signals of the Cretaceous bedrock and Northern China Craton, inherited from a river incision through Jihshan and Sanmen canyons (Stevens et al., 2013; Bird et al., 2015; Nie et al., 2015; Zhang et al., 2016). The contribution of debris from the Taihang Mountains to the lower Yellow River floodplain seems not significant as only a subdued component of the older zircon age population (1800–3000 Ma) has been seen in the lower reach of the Yellow River sediments.

Samples collected in the Sanmen Gorge area (Fig. 1) include fluvial sands of the Sanmen Formation (SM-Fm) with an age of 1.4 Ma (Kong et al., 2014), lacustrine sands (SM-lake) from the upper Sanmen palaeolake, and river terrace sands (SM-T3) from the third

terrace in Huangdigou (HDG, Fig. 1b) in the Sanmen Gorge. (Jiang et al., 2007). Sediments of the Sanmen Formation (Fig. 6f) show similar zircon age distribution pattern as that of the middle reach of the Yellow River, which has zircon age peaks at ca. 280 Ma, ca. 1850 Ma and ca. 2500 Ma. This suggests that the Yellow River has flowed through Sanmen Gorge since 1.4 Ma (Kong et al., 2014). The lacustrine sands of the Sanmen palaeolake (Fig. 6h) and the river terrace sample (SM-T3, Fig. 6g) also display a dominant zircon age peak at ca. 280 Ma, suggesting a major contribution of the middle reach of the Yellow River sediments. However, it is interesting to note that compared to the other samples from the Sanmen Gorge, the zircon age of the Sanmen palaeolake (SM-lake, Fig. 6h) and the river terrace sample (SM-T3, Fig. 6g) show an increase in the 350–550 Ma age population which is the dominant age component in sediments from the Wei River (Fig. 6e). Consistent with the age distribution patterns, the Sanmen palaeolake sample also lies close to the Wei River in the MDS map (Fig. 7). Based on the zircon provenance signal, Kong et al. (2014) concluded further that the Wei River primarily flowed through the Sanmen Gorge 1.3–1.5 Ma ago and then was followed by the Yellow River, which started to flow through the gorge from 1.3 to 1.4 Ma ago. As the time range provided by Kong et al. (2014) for the Yellow River and Wei River running through Sanmen Gorge largely overlap, it seems that both rivers flowed into the Sanmen palaeolake before it drained through Sanmen Gorge at around 1.3 Ma.

#### 4.3. Implications from the sedimentological and provenance variations of the Mangshan loess-palaeosol sequences

The zircon U-Pb age data reveal that provenance signals of the upper and the lower reaches of the Yellow River dominate the Mangshan loess deposits from L9 to L1 (~900 ka to 15 ka), implying that the lower Yellow River floodplain has consistently served as the main source supply for the MLP since 900 ka. This conclusion is in agreement with results from Pan (2005), Hu et al. (2012), Kong et al. (2014) and Hu et al. (2017), showing that the Yellow River has flown through Sanmen Gorge at least since the early Pleistocene. Therefore, the observed dramatic increases in Mangshan Loess grain size and sedimentation rate since S2 could result from (1) approaching of the source area or extension of the floodplain of the lower Yellow River, (2) an increased sediment supply from the lower Yellow River, or (3) an increased wind strength. Because the sedimentation rate and grain size below and above palaeosol unit S2 in the loess-palaeosol sequences from the CLP (Vandenberge et al., 1997; Ding et al., 2002; Sun, 2004; Sun and An, 2005; Sun et al., 2006) do not show a similar abrupt change as demonstrated in the Mangshan loess (Zheng et al., 2007), it is unlikely that winter monsoon intensity related wind strength changes played an important role. Thus, the sudden shift in sedimentology in the Mangshan sequence since 240 ka most probably arose from either the increased sediment supply of the lower Yellow River or the advance of its floodplain towards the MLP, or both.

Hu et al. (2012) found that the average incision rate of the Yellow River to the north of the Weihe Basin (Fig. 1b) increased dramatically since 240 ka as a result of local tectonic uplift. A recent study of the sedimentological infill of the Weihe Basin also suggests an increased incision rate of the fluvial system at approximately 240 ka resulting from enhanced tectonic activities (Rits et al., 2017). The finding suggests that differential tectonic movements in the Weihe Basin resulted in an increased sediment transfer propagating through the Sanmen Gorge. As a consequence, a wider alluvial fan system formed to the east of the Sanmen Gorge, next to the MLP (Fig. 1b). As this fan system served as a primary source for the MLP from ~240 ka onwards (Zheng et al., 2007), the accumulation rate on the plateau would have increased dramatically. An additional

tectonic explanation for the observed sedimentation rate increase is the migration of the lower Yellow River floodplain towards the Mangshan Plateau. The high scarp present along the northern and eastern limits of the MLP is the result of lateral erosion by river action, and evidences a southward migration of the lower Yellow River floodplain during the late Pleistocene. The migration provided a more proximal dust source area for the Mangshan loess deposits. The southward migration are probably induced by subtle vertical motions related to NW-SE directed faults in the subsurface (Hao et al., 2008; Zhang et al., 2008).

#### 5. Conclusions

The Mangshan loess-palaeosol record provides a high-resolution archive of dust supply from the Yellow River floodplain. The high accumulation rates, the coarse-grained character of the loess, and the distinct thinning and fining of the loess deposits in a north-south direction, clearly indicate increased coarser dust supply from the Yellow River floodplain to the Mangshan Plateau during the last two glacial-interglacial intervals. An independent provenance record by single grain zircon U-Pb ages confirms the lower Yellow River floodplain as the likely main source for the Mangshan dust deposits, at least since loess unit L9 (900 ka). This implies that the Yellow River incised the Sanmen Gorge before 900 ka (~MIS 22, i.e. late Early Pleistocene). The dramatic sedimentological change in the Mangshan sequences above S2 most likely originates from the tectonic activity in the Weihe Basin since 240 ka. This resulted in accelerated incision rate of the fluvial systems and associated release of eroded material through Sanmen Gorge towards the lower reach of the Yellow River floodplain. Meanwhile, a simultaneous southward migration and lateral erosion of the (lower) Yellow River resulted in a more proximal location of the dust source area, all contributing to increased loess deposition on the Mangshan Plateau during the late Pleistocene.

#### Acknowledgements

We thank Patrick Bacon, Xiangtong Huang, Ilse Kamerling, Simon Troelstra, Noortje Vromans, Ke Wang, Wieske Wentink, Hugo Wester, Wouter Wester, Bin Zhou and local farmers from the Liugou Village for their help with sampling the Mangshan loess-palaeosol sequences in 2006 and 2008. Roel van Elsas is thanked for supervision of heavy mineral separation. MAP and CJB thank the Royal Netherlands Academy of Arts and Sciences for financial support of these field projects. YS thanks the Doctoral Program of Geosciences of University of Helsinki for travel funding. BW acknowledges the Natural Science Foundation of China (Project Number 41602182) for financial support of the field work. We thank Xiaoping Yang for editorial work and two anonymous reviewers for their helpful and constructive reviews of the manuscript. This research is supported by the Academy of Finland grant to AK (Projects Numbers 257850, 264935 and 292827).

#### Appendix A. Supplementary data

Supplementary data related to this article can be found at <https://doi.org/10.1016/j.quascirev.2018.01.001>.

#### References

- AFSOM, 1988. Active Fault System Around Ordos Massif. Seismological Press, Beijing.
- An, Z.S., Kutzbach, J.E., Prell, W.L., Porter, S.C., 2001. Evolution of Asian monsoons and phased uplift of the Himalaya-Tibetan plateau since Late Miocene times. *Nature* 411, 62–66.
- Berger, A.L., 1978. Long-term variations of caloric insolation resulting from the

Earth's orbital elements. *Quat. Res.* 9, 139–167.

Bird, A., Stevens, T., Rittner, M., Vermeesch, P., Carter, A., Andò, S., Garzanti, E., Lu, H., Nie, J., Zeng, L., Zhang, H., Xu, Z., 2015. Quaternary dust source variation across the Chinese Loess Plateau. *Palaeogeogr. Palaeoclimatol. Palaeoecol.* 435, 254–264.

Cheng, H., Edwards, R.L., Broecker, W.S., Denton, G.H., Kong, X., Wang, Y., Zhang, R., Wang, X., 2009. Ice age terminations. *Science* 326, 248–252.

Cheng, H., Edwards, R.L., Sinha, A., Spotl, C., Yi, L., Chen, S., Kelly, M., Kathayat, G., Wang, X., Li, X., Kong, X., Wang, Y., Ning, Y., Zhang, H., 2016. The Asian monsoon over the past 640,000 years and ice age terminations. *Nature* 534, 640–646.

Deplazes, G., Lückge, A., Stütz, J.-B.W., Pätzold, J., Kuhlmann, H., Husson, D., Fant, M., Haug, G.H., 2014. Weakening and strengthening of the Indian monsoon during Heinrich events and Dansgaard-Oeschger oscillations. *Paleoceanography* 29, 99–114.

Derbyshire, E., Meng, X., Kemp, R.A., 1998. Provenance, transport and characteristics of modern aeolian dust in western Gansu Province, China, and interpretation of the Quaternary loess record. *J. Arid Environ.* 39, 497–516.

Ding, Z.L., Derbyshire, E., Yang, S.L., Sun, J.M., Liu, T.S., 2005. Stepwise expansion of desert environment across northern China in the past 3.5 Ma and implications for monsoon evolution. *Earth Planet. Sci. Lett.* 237, 45–55.

Ding, Z.L., Derbyshire, E., Yang, S.L., Yu, Z.W., Xiong, S.F., Liu, T.S., 2002. Stacked 2.6-Ma grain size record from the Chinese loess based on five sections and correlation with the deep-sea  $\delta^{18}\text{O}$  record. *Paleoceanography* 17. <https://doi.org/10.1029/2001PA000725>.

Hao, K., Tian, Q., Liu, B., Yin, G., 2008. Exploration of the Laoyachen fault, Zhengzhou of China, and its activity investigation. *Acta Seismol. Sin.* 30, 416–423.

Hu, Z., Pan, B., Bridgland, D., Vandenberghe, J., Guo, L., Fan, Y., Westaway, R., 2017. The linking of the upper-middle and lower reaches of the Yellow River as a result of fluvial entrenchment. *Quat. Sci. Rev.* 166, 324–338.

Hu, Z., Pan, B., Wang, J., Cao, B., Gao, H., 2012. Fluvial terrace formation in the eastern Fenwei Basin, China, during the past 1.2 Ma as a combined archive of tectonics and climate change. *J. Asian Earth Sci.* 60, 235–245.

Huang, C.C., Pang, J., Su, H., Li, S., Ge, B., 2009. Holocene environmental change inferred from the loess–palaeosol sequences adjacent to the floodplain of the Yellow River, China. *Quat. Sci. Rev.* 28, 2633–2646.

Ji, J.L., Zheng, H.B., Liu, R., Huang, X., Jiang, F.C., 2004. Restudy on the stratigraphy of Mangshan loess. *Mar. Geol. Quat. Geol.* 24, 101–108.

Jiang, F., Fu, J., Wang, S., Sun, D., Zhao, Z., 2007. Formation of the Yellow River, inferred from loess–palaeosol sequence in Mangshan and lacustrine sediments in Sanmen Gorge, China. *Quat. Int.* 175, 62–70.

Jiang, F.C., Wang, S.B., Zhao, Z.Z., Fu, J.L., 2004. Mangshan loess in Central China and the paleomonsoon variations since the last interglaciation. *Acta Geol. Sin.* 78, 813–819. <https://doi.org/10.1111/j.1755-6724.2004.tb00200.x>.

Jiang, F.C., Wu, X.H., Sun, D.H., Wang, S.M., An, Z.S., Tian, G.Q., Liu, K., Yin, W.D., Xue, B., 1998. On Mangshan loess stratigraphy in China central plains. *J. Geomech.* 4, 90–97.

Kohfeld, K.E., Harrison, S.P., 2003. Glacial-interglacial changes in dust deposition on the Chinese Loess Plateau. *Quat. Sci. Rev.* 22, 1859–1878.

Konert, M., Vandenberghe, J., 1997. Comparison of laser grain size analysis with pipette and sieve analysis: a solution for the underestimation of the clay fraction. *Sedimentology* 44, 523–535.

Kong, P., Jia, J., Zheng, Y., 2014. Time constraints for the Yellow River traversing the sanmen gorge. *Geochem. Geophys. Geosyst.* 15, 395–407. <https://doi.org/10.1002/2013GC004912>.

Kukla, G., 1987. Loess stratigraphy in central China. *Quat. Sci. Rev.* 6, 191–219.

Li, B., Sun, D., Xu, W., Wang, F., Liang, B., Ma, Z., Wang, X., Li, Z., Chen, F., 2017. Paleomagnetic chronology and paleoenvironmental records from drill cores from the Hetao Basin and their implications for the formation of the Hobq Desert and the Yellow River. *Quat. Sci. Rev.* 156, 69–89.

Licht, A., Pullen, A., Kapp, P., Abell, J., Giesler, N., 2016. Eolian cannibalism: reworked loess and fluvial sediment as the main sources of the Chinese Loess Plateau. *Geol. Soc. Am. Bull.* <https://doi.org/10.1130/B31375.1>. B31375.31371.

Lin, A., Yang, Z., Sun, Z., Yang, T., 2001. How and when did the Yellow River develop its square bend? *Geology* 29, 951–954.

Lisiecki, L.E., Raymo, M.E., 2005. A Pliocene-Pleistocene stack of 57 globally distributed benthic  $\delta^{18}\text{O}$  records. *Paleoceanography* 20. <https://doi.org/10.1029/2004PA001071>.

Liu, T., Ding, Z., 1998. Chinese loess and the paleomonsoon. *Annu. Rev. Earth Planet. Sci.* 26, 111–145.

Liu, T.S., 1985. Loess and the Environment. China Ocean Press, Beijing.

Lu, H.Y., Sun, D.H., 2000. Pathways of dust input to the Chinese Loess Plateau during the last glacial and interglacial periods. *Catena* 40, 251–261.

Nie, J., Stevens, T., Rittner, M., Stockli, D., Garzanti, E., Limonta, M., Bird, A., Andò, S., Vermeesch, P., Saylor, J., Lu, H., Breecker, D., Hu, X., Liu, S., Resentini, A., Vezzoli, G., Peng, W., Carter, A., Ji, S., Pan, B., 2015. Loess Plateau storage of Northeastern Tibetan Plateau-derived Yellow River sediment. *Nat. Commun.* 6, 8511. <https://doi.org/10.1038/ncomms9511>.

Nugteren, G., Vandenberghe, J., 2004. Spatial climatic variability on the Central Loess Plateau (China) as recorded by grain size for the last 250 kyr. *Global Planet. Change* 41, 185–206.

Pan, B., 2005. Paleomagnetic dating of the topmost terrace in Kouma, Henan and its indication to the Yellow River's running through Sanmen Gorges. *Chin. Sci. Bull.* 50, 657.

Pan, B., Hu, Z., Wang, J., Vandenberghe, J., Hu, X., 2011. A magnetostratigraphic record of landscape development in the eastern Ordos Plateau, China: Transition from Late Miocene and Early Pliocene stacked sedimentation to Late Pliocene and Quaternary uplift and incision by the Yellow River. *Geomorphology* 125, 225–238.

Peterse, F., Prins, M.A., Beets, C.J., Troelstra, S.R., Zheng, H., Gu, Z., Schouten, S., Damsté, J.S.S., 2011. Decoupled warming and monsoon precipitation in East Asia over the last deglaciation. *Earth Planet. Sci. Lett.* 301, 256–264.

Porter, S.C., 2001. Chinese loess record of monsoon climate during the last glacial–interglacial cycle. *Earth Sci. Rev.* 54, 115–128.

Prins, M.A., Postma, G., Weltje, G.J., 2000. Controls on terrigenous sediment supply to the Arabian Sea during the late Quaternary: the Makran continental slope. *Mar. Geol.* 169, 351–371.

Prins, M.A., Vriend, M., 2007. Glacial and interglacial eolian dust dispersal patterns across the Chinese Loess Plateau inferred from decomposed loess grain-size records. *Geochem. Geophys. Geosyst.* 8, Q07Q05. <https://doi.org/10.1029/2006GC001563>.

Prins, M.A., Vriend, M., Nugteren, G., Vandenberghe, J., Lu, H., Zheng, H., Jan Weltje, G., 2007. Late Quaternary aeolian dust input variability on the Chinese Loess Plateau: inferences from unmixing of loess grain-size records. *Quat. Sci. Rev.* 26, 230–242.

Prins, M.A., Weltje, G.J., 1999. End-member modeling of siliciclastic grain-size distributions: the Late Quaternary record of eolian and fluvial sediment supply to the Arabian Sea and its paleoclimatic significance. In: Harbaugh, J., Watney, L., Rankey, G., Slingerland, R., Goldstein, R., Franseen, E. (Eds.), *Numerical Experiments in Stratigraphy: Recent Advances in Stratigraphic and Sedimentologic Computer Simulations*, vol. 62. SEPM (Society for Sedimentary Geology) Special Publication, pp. 91–111.

Prins, M.A., Zheng, H., Beets, K., Troelstra, S., Bacon, P., Kamerling, I., Wester, W., Konert, M., Huang, X., Ke, W., Vandenberghe, J., 2009. Dust supply from river floodplains: the case of the lower Huang He (Yellow River) recorded in a loess–palaeosol sequence from the Mangshan Plateau. *J. Quat. Sci.* 24, 75–84.

Pye, K., 1995. The nature, origin and accumulation of loess. *Quat. Sci. Rev.* 14, 653–667.

Qiu, F., Zhou, L., 2015. A new luminescence chronology for the Mangshan loess–palaeosol sequence on the southern bank of the Yellow River in Henan, central China. *Quat. Geochronol.* 30, 24–33.

Rits, D.S., van Balen, R.T., Prins, M.A., Zheng, H., 2017. Evolution of the alluvial fans of the Luo River in the Weihe Basin, central China, controlled by faulting and climate change – a reevaluation of the paleogeographical setting of Dali Man site. *Quat. Sci. Rev.* 166, 339–351.

Shang, Y., Beets, C.J., Tang, H., Prins, M.A., Lahaye, Y., van Elsas, R., Sukselainen, L., Kaakinen, A., 2016. Variations in the provenance of the late Neogene Red Clay deposits in northern China. *Earth Planet. Sci. Lett.* 439, 88–100.

Shang, Y., Kaakinen, A., Beets, C.J., Prins, M.A., 2017. Aeolian silt transport processes as fingerprinted by dynamic image analysis of the grain size and shape characteristics of Chinese loess and Red Clay deposits. *Sediment. Geol.* <https://doi.org/10.1016/j.sedgeo.2017.12.001>.

Stacey, J.S., Kramers, J.D., 1975. Approximation of terrestrial lead isotope evolution by a two-stage model. *Earth Planet. Sci. Lett.* 26, 207–221.

Stevens, T., Carter, A., Watson, T.P., Vermeesch, P., Andò, S., Bird, A.F., Lu, H., Garzanti, E., Cottam, M.A., Sevastjanova, I., 2013. Genetic linkage between the Yellow River, the Mu Us desert and the Chinese Loess Plateau. *Quat. Sci. Rev.* 78, 355–368.

Stütz, J.-B.W., Prins, M.A., Schneider, R.R., Weltje, G.J., Jansen, J.H.F., Postma, G., 2002. A 300-kyr record of aridity and wind strength in southwestern Africa: inferences from grain-size distributions of sediments on Walvis Ridge, SE Atlantic. *Mar. Geol.* 180, 221–233.

Stütz, J.-B.W., Temmelsfeld, F., De Deckker, P., 2014. A 550 ka record of aeolian activity near North West Cape, Australia: inferences from grain-size distributions and bulk chemistry of SE Indian Ocean deep-sea sediments. *Quat. Sci. Rev.* 83, 83–94.

Sun, J., 2002. Provenance of loess material and formation of loess deposits on the Chinese Loess Plateau. *Earth Planet. Sci. Lett.* 203, 845–859.

Sun, D.H., 2004. Monsoon and westerly circulation changes recorded in the late Cenozoic aeolian sequences of Northern China. *Global Planet. Change* 41, 63–80.

Sun, D.H., Bloemendal, J., Rea, D.K., An, Z., Vandenberghe, J., Lu, H., Su, R., Liu, T., 2004. Bimodal grain-size distribution of Chinese loess, and its palaeoclimatic implications. *Catena* 55, 325–340.

Sun, D.H., Bloemendal, J., Rea, D.K., Vandenberghe, J., Jiang, F., An, Z., Su, R., 2002. Grain-size distribution function of polymodal sediments in hydraulic and aeolian environments, and numerical partitioning of the sedimentary components. *Sediment. Geol.* 152, 263–277.

Sun, Y., An, Z., 2005. Late Pliocene–Pleistocene changes in mass accumulation rates of aeolian deposits on the central Chinese Loess Plateau. *J. Geophys. Res. Atmos.* 110, D23101.

Sun, Y., Chen, J., Clemens, S.C., Liu, Q., Ji, J., Tada, R., 2006. East Asian monsoon variability over the last seven glacial cycles recorded by a loess sequence from the northwestern Chinese Loess Plateau. *Geochem. Geophys. Geosyst.* 7, Q12Q02. <https://doi.org/10.1029/2006GC001287>.

Van Achterbergh, E., Ryan, C., Jackson, S., Griffin, W., 2001. Data reduction software for LA-ICP-MS. In: P. S. (Ed.), *Laser-ablation ICPMS in the Earth Sciences – Principles and Applications*. Mineralogical Association of Canada Short Course Series, St John, Newfoundland, pp. 239–243.

Vandenberghe, J., An, Z.S., Nugteren, G., Lu, H.Y., van Huissteden, J., 1997. New absolute time scale for the Quaternary climate in the Chinese loess region by

grain-size analysis. *Geology* 25, 35–38.

Vermeesch, P., 2013. Multi-sample comparison of detrital age distributions. *Chem. Geol.* 341, 140–146.

Vermeesch, P., Resentini, A., Garzanti, E., 2016. An R package for statistical provenance analysis. *Sediment. Geol.* 336, 14–25.

Vriend, M., Prins, M.A., Buylaert, J.P., Vandenbergh, J., Lu, H.Y., 2011. Contrasting dust supply patterns across the north-western Chinese Loess Plateau during the last glacial-interglacial cycle. *Quat. Int.* 240, 167–180.

Wang, S., 2002. Sedimentary records of environmental evolution in the Sanmen Lake Basin and the Yellow River running through the Sanmenxia Gorge eastward into the sea. *Sci. China Earth Sci.* 45, 595–608.

Wang, S., Fu, B., Piao, S., Lü, Y., Ciais, P., Feng, X., Wang, Y., 2015. Reduced sediment transport in the Yellow River due to anthropogenic changes. *Nat. Geosci.* 9, 38–41.

Wang, S.B., Jiang, F.C., Fu, J.L., Li, C.Z., Cai, Y., Yao, H.T., Qiao, Y.S., Zhang, Z.S., Li, Y.J., 2013. Some knowledge of the formation of the Yellow River. *Quat. Sci.* 33, 705–714.

Wang, Y., Cheng, H., Edwards, R.L., Kong, X., Shao, X., Chen, S., Wu, J., Jiang, X., Wang, X., An, Z., 2008. Millennial- and orbital-scale changes in the East Asian monsoon over the past 224,000 years. *Nature* 451, 1090–1093.

Weltje, G.J., 1997. End-member modeling of compositional data: numerical-statistical algorithms for solving the explicit mixing problem. *Math. Geol.* 29, 503–549.

Weltje, G.J., Prins, M.A., 2003. Muddled or mixed? Inferring palaeoclimate from size distributions of deep-sea clastics. *Sediment. Geol.* 162, 39–62.

Weltje, G.J., Prins, M.A., 2007. Genetically meaningful decomposition of grain-size distributions. *Sediment. Geol.* 202, 409–424.

Wu, X., Jiang, F., Xiao, H., Xue, B., Sun, D., 1999. Mangshan loess on China's Central Plain and its response to tectonic movement and climate. *Sci. China Earth Sci.* 42, 465–473. <https://doi.org/10.1007/BF02875240>.

Xiao, J., Chang, Z., Si, B., Qin, X., Itoh, S., Lomtatidze, Z., 2009. Partitioning of the grain-size components of Dali Lake core sediments: evidence for lake-level changes during the Holocene. *J. Paleolimnol.* 42, 249–260.

Xiao, J., Fan, J., Zhou, L., Zhai, D., Wen, R., Qin, X., 2013. A model for linking grain-size component to lake level status of a modern clastic lake. *J. Asian Earth Sci.* 69, 149–158.

Zhang, H., Lu, H., Xu, X., Liu, X., Yang, T., Stevens, T., Bird, A., Xu, Z., Zhang, T., Lei, F., Feng, H., 2016. Quantitative estimation of the contribution of dust sources to Chinese loess using detrital zircon U-Pb age patterns. *J. Geophys. Res. Earth Surf.* 121, 2085–2099.

Zhang, J., Shen, J., Tian, Q., Shen, X., Zhang, X., Li, B., 2008. Relationship between Mangshan geomorphic scarp and Laoyachen fault activity. *Earthquake* 28, 121–127.

Zheng, H., Huang, X., Ji, J., Liu, R., Zeng, Q., Jiang, F., 2007. Ultra-high rates of loess sedimentation at Zhengzhou since stage 7: implication for the Yellow River erosion of the Sanmen Gorge. *Geomorphology* 85, 131–142.